

Electrically induced cancellation and inversion of piezoelectricity in ferroelectric $\text{Hf}_{0.5}\text{Zr}_{0.5}\text{O}_2$

Received: 12 August 2023

Accepted: 30 December 2023

Published online: 29 January 2024

 Check for updates

Haidong Lu^{1,7}, Dong-Jik Kim^{2,7}, Hugo Aramberrí³, Marco Holzer^{2,4}, Pratyush Buragohain¹, Sangita Dutta^{3,5}, Uwe Schroeder⁶, Veeresh Deshpande², Jorge Íñiguez^{3,5} ✉, Alexei Gruverman¹ ✉ & Catherine Dubourdieu^{2,4} ✉

HfO_2 -based thin films hold huge promise for integrated devices as they show full compatibility with semiconductor technologies and robust ferroelectric properties at nanometer scale. While their polarization switching behavior has been widely investigated, their electromechanical response received much less attention so far. Here, we demonstrate that piezoelectricity in $\text{Hf}_{0.5}\text{Zr}_{0.5}\text{O}_2$ ferroelectric capacitors is not an invariable property but, in fact, can be intrinsically changed by electrical field cycling. $\text{Hf}_{0.5}\text{Zr}_{0.5}\text{O}_2$ capacitors subjected to ac cycling undergo a continuous transition from a positive effective piezoelectric coefficient d_{33} in the pristine state to a fully inverted negative d_{33} state, while, in parallel, the polarization monotonically increases. Not only can the sign of d_{33} be uniformly inverted in the whole capacitor volume, but also, with proper ac training, the net effective piezoresponse can be nullified while the polarization is kept fully switchable. Moreover, the local piezoresponse force microscopy signal also gradually goes through the zero value upon ac cycling. Density functional theory calculations suggest that the observed behavior is a result of a structural transformation from a weakly-developed polar orthorhombic phase towards a well-developed polar orthorhombic phase. The calculations also suggest the possible occurrence of a non-piezoelectric ferroelectric $\text{Hf}_{0.5}\text{Zr}_{0.5}\text{O}_2$. Our experimental findings create an unprecedented potential for tuning the electromechanical functionality of ferroelectric HfO_2 -based devices.

The discovery of ferroelectricity in hafnium oxide (HfO_2) thin films opened exciting opportunities for their monolithic integration with the existing complementary metal-oxide-semiconductor (CMOS) technology^{1,2}. Ever since the first report of ferroelectricity in Si-doped

HfO_2 (Si:HfO_2)¹, there have been concerted efforts towards understanding the origin of ferroelectricity in hafnium oxide^{3–10}. Ferroelectricity has been primarily attributed to a polar orthorhombic phase (space group $Pca2_1$, noted o-III phase)^{4,5,11}, although a polar

¹Department of Physics and Astronomy, University of Nebraska-Lincoln, Lincoln, NE 68588-0299, USA. ²Helmholtz-Zentrum Berlin für Materialien und Energie, Insitute Functional Oxides for Energy-Efficient Information Technology, Hahn Meitner Platz 1, 14109 Berlin, Germany. ³Materials Research and Technology Department, Luxembourg Institute of Science and Technology (LIST), Avenue des Hauts-Fourneaux 5, L-4362 Esch/Alzette, Luxembourg. ⁴Freie Universität Berlin, Physical and Theoretical Chemistry, Arnimallee 22, 14195 Berlin, Germany. ⁵Department of Physics and Materials Science, University of Luxembourg, Rue du Brill 41, L-4422 Belvaux, Luxembourg. ⁶NaMLab gGmbH, Noethnitzer Strasse 64 a, 01187 Dresden, Germany. ⁷These authors contributed equally: Haidong Lu and Dong-Jik Kim. ✉ e-mail: jorge.iniguez@list.lu; agruverman2@unl.edu; catherine.dubourdieu@helmholtz-berlin.de

rhombohedral phase ($R3m$, r-phase) has also been experimentally reported⁷ and at least five polar phases have been predicted by density functional theory (DFT)¹². Due to the relatively small energy differences between the various polymorphs of HfO_2 , there can be phase coexistence of centrosymmetric monoclinic ($P2_1/c$, m-phase) and tetragonal ($P4_2/mnc$, t-phase) phases along with the polar non-centrosymmetric phases in the polycrystalline HfO_2 films, leading to a complex system that is highly sensitive to the growth conditions, doping concentration, strain, film thickness, electrodes, etc.^{3,10,13–17}. Consequently, complex behaviors such as antiferroelectricity in t-phase rich films^{2,3}, field-induced phase transformations and enhanced ferroelectricity with field cycling^{11,18,19}, interplay between depolarization field and wake-up effects²⁰, are frequently observed in HfO_2 -based ferroelectric (FE) systems. In addition, several intriguing features, such as the disputed nature of ferroelectricity^{9,21–23}, enhancement of ferroelectricity at reduced dimensions², negative domain wall energies^{9,24} and negative longitudinal piezoelectric coefficient, d_{33} ^{25–28}, make hafnia ferroelectrics a unique and fascinating class of materials to study.

The potential of FE HfO_2 towards technological applications has been demonstrated already through the realization of ferroelectric field effect transistors (FeFETs)²⁹, 3-dimensional trench capacitors with high endurance³⁰, negative capacitance-based devices that allow transistors to overcome “Boltzmann’s tyranny”³¹, ferroelectric tunnel junctions (FTJs) for resistive switching^{32–34} and neuromorphic computing applications^{35–37}. The recent surge of interest in the piezoelectric properties of these materials stems from the emerging controversy between the theoretical and experimental data. Several theoretical reports have predicted a negative longitudinal piezoelectric coefficient d_{33} ^{25–27}, which arises from the peculiar chemical environment of the oxygen atoms. However, the majority of the experimental works have demonstrated a positive d_{33} ^{38–41}. Only recently, a few experimental demonstrations of negative d_{33} in HfO_2 have been reported^{27,28,42}. Moreover, it has been observed that the sign of the d_{33} could vary depending on the film thickness, electrode materials, and deposition method used^{38–42}. In addition, the coexistence of regions with positive and negative d_{33} piezoelectric coefficients within the same device has been reported⁴².

From the experimental point of view, the sign of the piezoelectric coefficient determines whether the ferroelectric sample expands or contracts under an applied electric field—a phenomenon known as the converse piezoeffect. One of the most common methods to investigate this phenomenon is piezoelectric force microscopy (PFM). This technique employs a conductive nanoscopic tip under an electrical bias to probe the local electromechanical response of the sample at the scale range of several nanometers, thereby providing information on

the local piezoelectric properties⁴³. Application of PFM has revealed the existence of regions in the $\text{Hf}_{0.5}\text{Zr}_{0.5}\text{O}_2$ (HZO) films that were apparently switching against the external electric field, as was deduced from monitoring the change in the PFM phase signal^{42,44}. However, careful analysis of the calibrated piezoresponse signal demonstrated that this apparently abnormal switching behavior was, in fact, a manifestation of the regions with positive d_{33} coefficient within the negative d_{33} matrix⁴².

Here, we show that the sign of piezoelectricity in the HZO films can be changed by an electrical field and, in addition, that piezoelectricity can be nullified while keeping robust switchable polarization. PFM imaging of the W/HZO/W capacitors subjected to ac cycling revealed a gradual transition from a uniformly positive d_{33} state in the pristine capacitors to a fully inverted uniform negative d_{33} state (while, in parallel, the polarization monotonically increases by about 20%). At some intermediate stage along this evolution, the HZO capacitors exhibit a zero net piezoelectricity due to coexisting positive and negative d_{33} regions while displaying fully switchable polarization. Local PFM spectroscopy provides an additional insight into this process by displaying a gradual reduction of the positive d_{33} value, and then a gradual increase in the d_{33} value but with a negative sign. Remarkably, every single location of the capacitor goes through zero local piezoelectricity upon ac cycling. DFT calculations investigating the path from the non-polar tetragonal phase to the ferroelectric o-III phase reveal an unprecedented non-monotonic behavior of the strain with the development of polarization. Hence, the simulations suggest that the initial positive d_{33} sign and sizeable remanent polarization ($\geq 19 \mu\text{C}/\text{cm}^2$) in the pristine state can be attributed to a weakly-developed polar orthorhombic phase that, upon ac cycling, progressively evolves towards a well-developed polar o-III phase with negative d_{33} .

Results

Ferroelectricity switching in W/HZO/W capacitors

Figure 1a shows typical polarization versus voltage loops measured on the W/HZO/W capacitors as a function of ac electrical cycling (the corresponding I - V curves are shown in Fig. S1 of the Supplementary Information). Additional examples of P - V loops upon cycling are given in the Supplementary Information. In the pristine state, a remanent polarization P_r of $19.0 \mu\text{C}/\text{cm}^2$ is observed, and the hysteresis loop is closed and saturated (whereas pinched hysteresis loops are frequent in pristine HZO capacitors with TiN electrodes). Continuing ac cycling results in a further increase of the remanent polarization, which reaches $21.5 \mu\text{C}/\text{cm}^2$ after 2000 cycles and $22.2 \mu\text{C}/\text{cm}^2$ after 30,000 cycles (Fig. 1b). Considering all samples/capacitors studied, P_r is typically of 19 – $23 \mu\text{C}/\text{cm}^2$ in the pristine state, of 22 – $28 \mu\text{C}/\text{cm}^2$ after 10^4

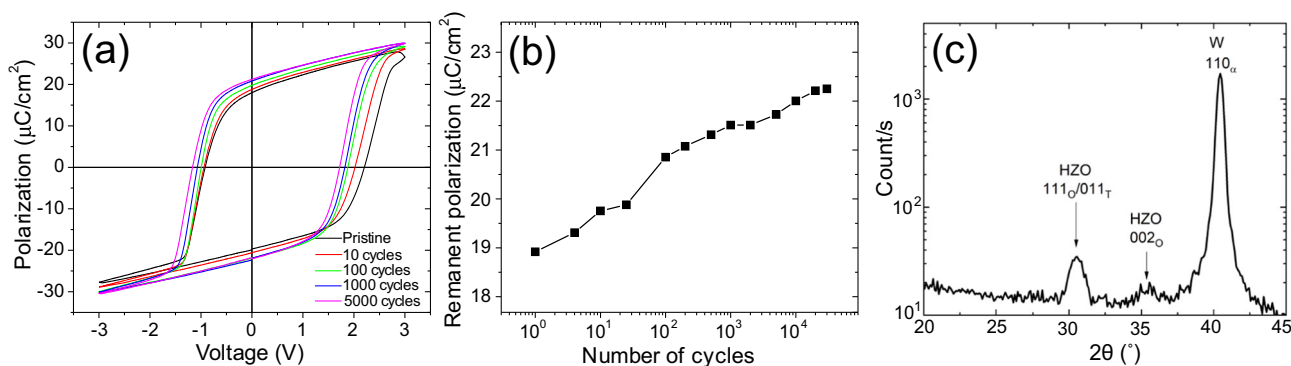


Fig. 1 | Ferroelectric switching and X-ray diffraction data. **a** Polarization hysteresis loops versus the set voltage of a W/HZO/W capacitor in the pristine state and after various numbers of ac field cycles. **b** Remanent polarization (average of P_r^+

and P_r^-) as a function of the ac cycles. **c** Grazing incidence X-ray diffraction pattern of the pristine sample (W/HZO/W with full W top sheet layer).

cycles and of $\sim 30 \mu\text{C}/\text{cm}^2$ after 10^5 cycles. The P_r values are similar to those reported for HZO stacks with a top W electrode^{45,46}. The HZO capacitors with bottom and top W electrodes are almost wake-up free, which is significantly different from other polycrystalline HfO_2 -based ferroelectric capacitors, which require a wake-up phase of typically ~ 1000 – 2000 field cycles to reach open saturated loops and close to full remanent polarization^{11,17,34,47–49}. Wake-up-free behavior with W top and bottom electrodes has been previously reported¹⁴⁶. The fact that P_r in the pristine state is already quite large indicates that the pristine film contains a large portion of polar phase. From the X-ray diffraction patterns of the pristine samples, no monoclinic phase is observed (Fig. 1c). A typical peak is recorded at $2\theta \sim 30.5^\circ$, which can be assigned to the tetragonal and/or polar o-III orthorhombic phase. Since the peak width depends on the grain size and on the microstrain in the film, it is not possible to unambiguously assign this peak to one phase (o-III) or to a mixture of t and o-III phases. We also observe the 002 peak of the o-III phase.

Inversion of the net piezoresponse signal upon ac cycling

Figure 2 shows a series of PFM phase images recorded in the same location of a poled W/HZO/W capacitor at different stages of the ac training process. The measurement conditions are specified in the Methods section. After the application of a certain number of the field cycles, the capacitors were poled by the application of positive or negative voltage pulses with an amplitude well above the coercive voltage. The PFM images of the pristine capacitor (Fig. 2a, b) reveal uniform contrast after poling, indicating a fully switchable polarization. This result is consistent with the large remanent polarization in the pristine state observed in the macroscopic P - V loop measurement (Fig. 1a, black curve). Analysis of the calibrated PFM phase signal⁴² of the capacitor poled to the downward polarization state (appearing with dark contrast in the PFM image (Fig. 2a)) suggests that it oscillates in-phase with the ac drive signal (i.e., the capacitor expands under a positive bias). Correspondingly, the oscillation of the pristine capacitor poled upward (appearing with bright contrast in PFM (Fig. 2b)) is out-of-phase with the ac drive signal (the capacitor contracts under a positive bias). This is an indication of a positive, effective piezocoefficient d_{33} in the pristine HZO. However, ac cycling leads to the appearance of regions with an inverted PFM response after poling: these regions exhibit an out-of-phase PFM signal (bright contrast) after positive pulse application and, correspondingly, in-phase signal (dark contrast) after a negative pulse (Fig. 2c,d). Although the emergence of the regions with an inverted PFM response appears as polarization switching against the applied field (the so-called “anomalous” switching), PFM phase signal analysis gives a very clear indication that these regions exhibit a negative d_{33} piezocoefficient. The area occupied by the regions with negative d_{33} continuously increases as a function of ac

training (Fig. 2e–j). After 5000 cycles, more than 95% of the capacitor area shows an inverted PFM phase contrast in comparison to the pristine state (Fig. 2k, l). Full d_{33} inversion requires typically 1000–5000 cycles, depending on the capacitor. The net zero piezoresponse of the whole capacitor (Fig. 2m and Fig. S2 of the Supplementary Information) results from the coexistence of positive and negative d_{33} regions. It is remarkable to note that the capacitor keeps a robust and fully switchable polarization (Fig. 1b and Fig. S2g) when its net piezoresponse is null.

Inversion of the local piezoresponse signal upon ac cycling

To further explore the evolution of the piezoresponse with ac training, local PFM switching spectroscopy loops were collected at several locations. Figure 3a–f shows the evolution of the representative bias-off PFM loops with an increasing number of ac switching cycles. In the pristine state, the PFM testing reveals a conventional hysteretic loop corresponding to a positive piezoelectric coefficient (Fig. 3a). The PFM signal decreases in magnitude after 25 cycles of ac training (Fig. 3b) and after 100 cycles the PFM hysteresis loop appears as mirror-reflected indicating an inversion of the PFM signal, which is still of low magnitude (Fig. 3c). Further ac training increases the PFM signal magnitude and eventually results in a hysteretic loop corresponding to the negative piezoelectric coefficient (Fig. 3d–f). This gradual change of the PFM spectroscopy loop as a function of ac training cycles suggests that the inversion of the d_{33} coefficient at the local level is not instantaneous but rather gradual: from a positive d_{33} through a continuous reduction of its magnitude going through zero, followed by its sign inversion and then a gradual increase of the negative d_{33} value. This is illustrated in Fig. 3g for two different locations of a capacitor measured after a very progressive ac cycling to follow closely the evolution of the electromechanical response (the piezoresponse amplitude and phases are shown in Fig. S3 of the Supplementary Information). Hence, not only can the net piezoresponse of the whole capacitor be nullified, but also the local piezoresponse. Depending on the location of the capacitor, the nullification of the electromechanical response occurs for an ac cycling of tens to thousands of cycles. The P - V loops measured after each applied ac cycle show a non-zero polarization of the capacitor. While we cannot ascertain the existence of a switchable polarization at the local scale when the local d_{33} is nullified, it is most plausible to assume that the local polarization does not suddenly go to zero while being a robust one ($>20 \mu\text{C}/\text{cm}^2$) just before and after the nullification. Note that the tip-sample contact radius is estimated to not exceed 15 nm, which implies that a maximum of 2–3 grains are involved in each of the local switching spectroscopy measurements.

To check if a local back-switching effect (for example, due to the presence of an internal built-in field) takes place upon removal of the

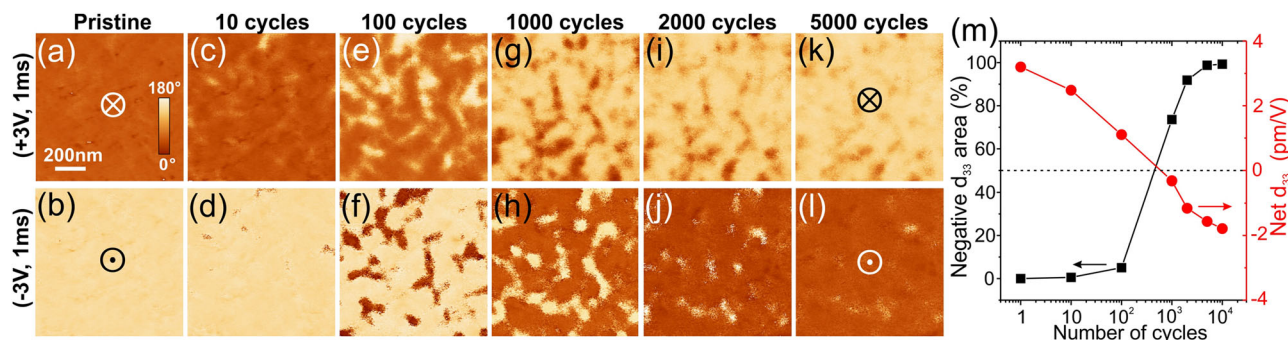


Fig. 2 | PFM imaging of a poled W/HZO/W capacitor as a function of the ac cycling. a–l PFM phase images representing the domain structures after application of the positive (top row) and negative (bottom row) poling pulses collected in the same location: (a, b) pristine state, (c, d) after 10 cycles, (e, f) 100 cycles, (g, h)

1000 cycles, (i, j) 2000 cycles, and (k, l) 5000 cycles. Pulse amplitude is ± 3 V, and duration is 1 ms. m Percentage of the area with negative piezocoefficient d_{33} and the average d_{33} value of the entire scanned area as a function of ac cycling obtained from image analysis of data in (a, c, e, g, i, k).

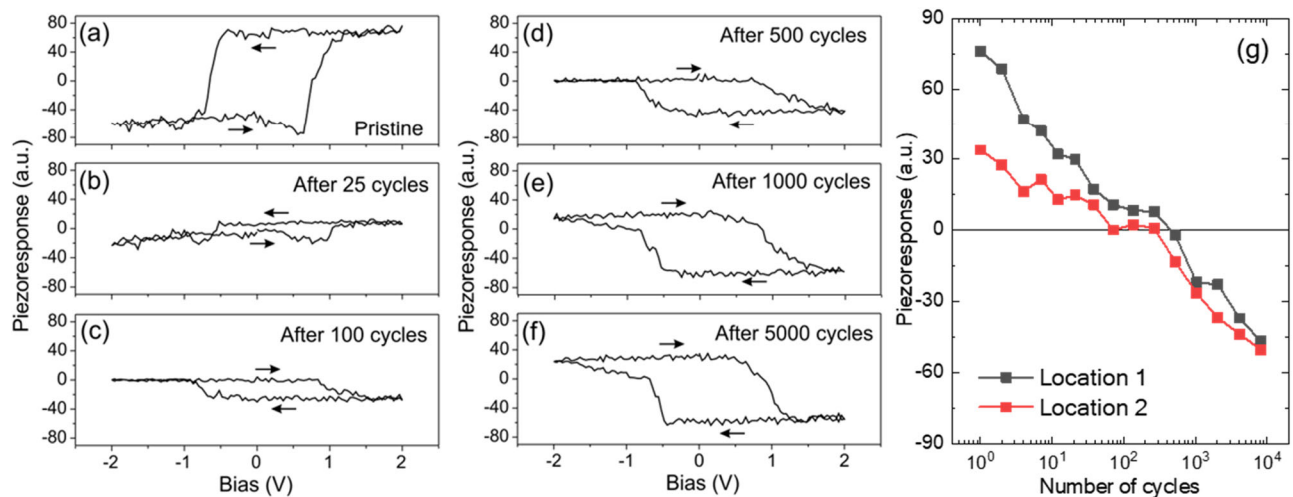


Fig. 3 | PFM switching spectroscopy at a fixed location on a W/HZO/W capacitor as a function of the ac cycling process. **a–f** Bias-off piezoresponse loops in the pristine state **(a)**, after 25 cycles **(b)**, 100 cycles **(c)**, 500 cycles **(d)**, 1000 cycles **(e)**, and 5000 cycles of ac cycling **(f)**, respectively. The piezoresponse loops were

obtained by convoluting the PFM amplitude signal with the cosine of the PFM phase signal. **g** Local PFM amplitude evolution as a function of the number of ac cycles at two different locations of a capacitor (the bias-off PFM amplitude and phase loops are shown in Fig. S3 of the Supplementary Information).

dc poling voltages, the PFM switching spectroscopy loops were also collected simultaneously in the bias-on regime, where the piezoresponse signal was recorded in the presence of the dc bias (Fig. S4 of the Supplementary Information). The results are qualitatively similar to those shown in Fig. 3. The obtained data suggest that back-switching can be ruled out as a possible cause of the observed PFM phase inversion.

Origin of the piezoelectric coefficient sign inversion and cancellation

Let us now discuss the possible mechanism at the origin of the inversion of the piezoelectric coefficient sign in the ferroelectric HZO upon electrical cycling. The full inversion of the d_{33} sign (on a $1 \times 1 \mu\text{m}^2$ area) is observed typically after 2000 ac cycles (we give additional examples for a different sample in Fig. S3 of the Supplementary Information). The W/HZO/W capacitors just after one ac cycle show closed saturated hysteresis loops. After 2000 cycles, the remanent polarization P_r increases typically by 5–25% and keeps slowly increasing up to at least 10,000 cycles while full inversion of d_{33} in the capacitor has already occurred (Fig. S3B, C). The d_{33} inversion does not seem to be related to the standard wake-up mechanisms^{11,49}. Extrinsic phenomena invoked^{18,50} such as charge detrapping or charge redistribution, decrease of depolarization field, and domain wall depinning, cannot account for a change of the sign of d_{33} . Moreover, the careful calibration based on the procedure described in⁴² allows us to rule out or account for the parasitic effects of any extrinsic phenomena on the measured electromechanical response. The influence of imprint on the piezoresponse could be questioned. Although in Fig. 1 we indeed observe a reduction of the coercive voltage V_c^+ by ~ 0.5 V after 5000 ac cycles, the vast majority of our capacitors (tested on different samples) exhibit, however, negligible change of the imprint, as we show in Fig. S5. The coercive voltage V_c^+ increases typically by 0.2 V over the first three to ten cycles and then remains constant (Fig. S5). The imprint window varies by less than 0.1 V upon the 10,000 cycles. Hence, we can confidently exclude that phenomena related to imprint (such as charge redistribution) account for the sign change of d_{33} . Electrical cycling during the wake-up phase has also been suggested to trigger a crystalline phase transition from the non-ferroelectric monoclinic or tetragonal $P4_2/nmc$ to the polar orthorhombic $Pca2_1$ phase via oxygen vacancy migration^{11,51,52}. Here, we can rule out that the capacitors contain a majority of non-ferroelectric phase(s). No

monoclinic phase is observed by X-ray diffraction, and in view of the high remanent polarization P_r ($>20 \mu\text{C}/\text{cm}^2$) reached in the pristine state or just after 1 cycle, we can rule out that the capacitors contain a majority of tetragonal phase. At any rate, note that a high volume fraction of the centrosymmetric ($d_{33} = 0$) tetragonal or monoclinic phases in the pristine samples would result in a weaker piezoelectric effect but cannot yield a change of sign.

We now resort to first-principles simulations to discuss whether it is possible to explain the observed sign reversal of d_{33} by an *intrinsic* physical mechanism, i.e., present in a perfect HZO lattice, not related to defects or interfacial phenomena. As previously discussed in the introduction, the piezoelectric response of the usual ferroelectric phase of HfO_2 (orthorhombic, $Pca2_1$ space group) is qualitatively different from the response of the best-known piezoelectrics (i.e., perovskite oxides like PbTiO_3 or $\text{PbZr}_{1-x}\text{Ti}_x\text{O}_3$)²⁷. In particular, the longitudinal piezoresponse is negative in HfO_2 , implying that compression along the polar direction results in an enhancement of the polarization; indeed, we compute a negative $e_{33} = -144 \mu\text{C}/\text{cm}^2$. It has been shown that this peculiar behavior stems from the chemical environment of the active oxygens that drive the occurrence of spontaneous polarization. In this work, we have run a similar DFT investigation for HZO as well as pure ZrO_2 , both considered in a $Pca2_1$ configuration analogous to HfO_2 's ferroelectric state. For HZO, here we present results for the particular Hf/Zr ordering shown in Fig. S6a of the Supplementary Information (we considered alternative Hf/Zr arrangements—also shown in Fig. S6—and explicitly checked that the dependence of e_{33} on the cation order is negligible ($<2\%$)). We obtain a theoretical spontaneous polarization of about $55 \mu\text{C}/\text{cm}^2$ for both materials, essentially identical to the result for HfO_2 . As for e_{33} , we obtain $-159 \mu\text{C}/\text{cm}^2$ for HZO and $-174 \mu\text{C}/\text{cm}^2$ for ZrO_2 , confirming that the negative linear piezoresponse is a general feature of this polar state, the magnitude of the effect being weakly dependent on composition. Thus, our DFT calculations are compatible with the negative d_{33} observed in our samples upon cycling.

What can then be the origin of the positive d_{33} measured in the pristine samples? Our simulations suggest two possible explanations based on intrinsic mechanisms. On the one hand, we find that in these materials the sign of the longitudinal piezoresponse depends strongly on the extent to which the spontaneous polarization is developed. Our key first-principles results, summarized in Fig. 4, are obtained in the following way: we consider the paraelectric t-phase as a reference

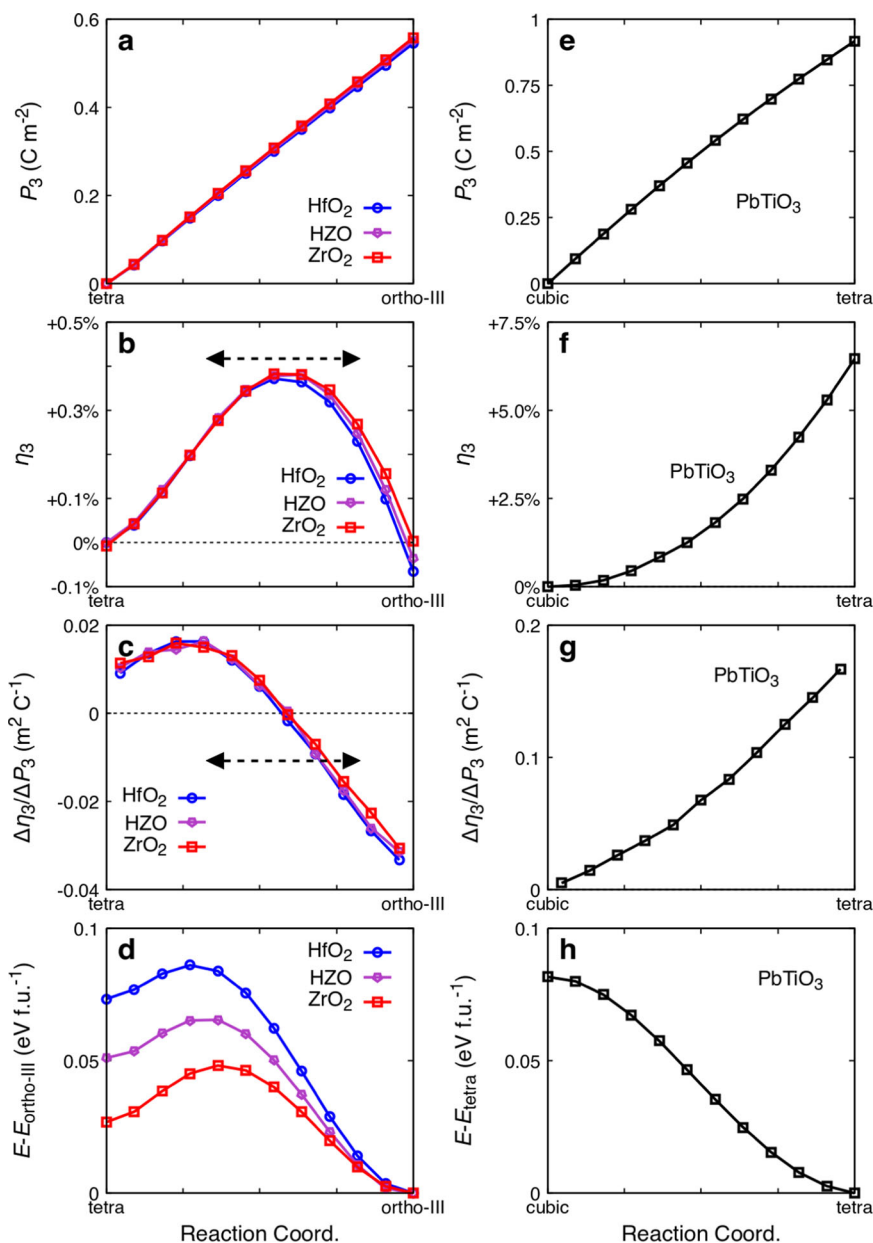


Fig. 4 | Predicted nontrivial piezoresponse of hafnia ferroelectrics. Connection between polarization P_3 and strain along the polar axis η_3 , as computed for HfO₂, HZO, and ZrO₂ (a–d) and PbTiO₃ (e–h). The “Reaction Coordinate” in the horizontal axis refers to a linear structural interpolation between a paraelectric reference state (tetragonal for HfO₂, HZO, and ZrO₂; cubic for PbTiO₃) and the ferroelectric state (orthorhombic $Pca2_1$ o-III phase for HfO₂, HZO and ZrO₂; tetragonal for PbTiO₃). a, e show the polarization of the different materials, while b and f show the corresponding evolution of η_3 . c, g show the ratio $\Delta\eta_3/\Delta P_3$ along the reaction coordinate, which roughly goes as the d_{33} piezoelectric coefficient (in essence,

$d_{33} \sim \epsilon_0 \chi_{33} \Delta\eta_3/\Delta P_3$, where ϵ_0 is the vacuum’s permittivity and χ_{33} the relevant dielectric susceptibility). d, h show the energy of the different phases as a function of the reaction coordinate, taking the polar minimum as the zero of energy. Noting the simplifications implicit in our simulations, in b, c we mark with dashed double arrows the approximate region where we expect d_{33} to change sign. Interestingly, this range roughly overlaps with the one defined by the smallest ($\sim 19\text{--}23 \mu\text{C}/\text{cm}^2$ in the pristine state) and largest ($30 \mu\text{C}/\text{cm}^2$ after 10^5 cycles) remnant polarizations experimentally measured in our samples.

structure, and simulate several configurations that can be viewed as a structural interpolation between this non-polar state and the o-III ferroelectric phase. Such intermediate configurations are constructed by displacing the atoms from the reference state as required to reach the polar configuration; the relative positions of the atoms are then fixed, and the cell strains (lattice vectors) are optimized so they can adapt to the progressive development of the orthorhombic $Pca2_1$ (polar) distortion. Thus, while the evolution of the polarization P_3 (Fig. 4a) is imposed by hand in these calculations, the cell strain along the polar axis, η_3 (Fig. 4b), is a result of the DFT optimization. Surprisingly, we find that η_3 does not follow the polarization monotonically; instead,

the strain grows when the polarization starts condensing, reaches a maximum (when about 60% of the full theoretical polarization has developed), and decays beyond that point. Since d_{33} is essentially given by the ratio of the strain and polarization changes (Fig. 4c), our results suggest that this coefficient will reverse its sign, from positive to negative, in a continuous way as the distortion develops. Note that this is a unique feature of HfO₂ and related materials: our analogous results for PbTiO₃ (Fig. 4e–h) illustrate the behavior that is typical of ferroelectric perovskites, namely, a monotonic development of η_3 with P_3 , yielding $d_{33} > 0$ throughout the condensation of the polar distortion. The peculiarity of HfO₂-related compounds is further reflected in

the complex energy landscape (Fig. 4d) connecting the paraelectric and ferroelectric ortho-III phases, which contrasts with the simplicity we find in PbTiO_3 (Fig. 4h).

From Fig. 4a, b, we find that the calculated maximum of η_3 for HZO corresponds to a polarization of $-33 \mu\text{C}/\text{cm}^2$, which nearly falls within the range of polarization values measured in our capacitors in their pristine state (typically between 19 and $23 \mu\text{C}/\text{cm}^2$), and after 10^5 cycles ($30 \mu\text{C}/\text{cm}^2$). Note that, given the structural complexity of the HZO samples (grains, grain boundaries, phase coexistence, point and linear defects) we can hardly expect a good quantitative agreement in polarization between experiment and theory when simulating an ideal system. Hence, our simulations suggest that our pristine capacitors should present a positive d_{33} ; further, our calculations indicate that, upon cycling, d_{33} can be expected to decrease in magnitude and even become negative. Hence, notwithstanding the differences between our ideal simulated crystals and the actual polycrystalline samples, this unique predicted behavior of HfO_2 , HZO and ZrO_2 —i.e., the non-monotonic relationship between polarization and strain—provides a plausible intrinsic explanation to the surprising sign inversion of d_{33} observed experimentally. The evolution along the calculated path under ac cycling can be attributed to the progressive development of the polar distortion of the o-III phase. The calculations remarkably account not only for the inversion of the d_{33} sign but also for its behavior as observed in switching spectroscopy (Fig. 3): a continuous decrease in magnitude, going through zero, followed—after its sign inversion—by a gradual increase.

On the other hand, HfO_2 -related compounds present many polymorphs¹², which suggests the following alternative scenario: our HZO samples might be grown in a different ferroelectric structure (with $d_{33} > 0$), then transform into the commonly assumed orthorhombic $Pca2_1$ polymorph (with $d_{33} < 0$) upon cycling. In particular, the theoretical literature on HfO_2 has discussed a second ferroelectric orthorhombic phase (noted “ortho-IV” in the following, with $Pmn2_1$ space group), which would be a potential candidate to appear in our as-grown films^{12,53}. Both orthorhombic HfO_2 polar phases have been found to have similar spontaneous polarizations ($P_{Pca2_1} = 52 \mu\text{C}/\text{cm}^2$ and $P_{Pmn2_1} = 56 \mu\text{C}/\text{cm}^2$)¹². We have run a standard DFT characterization of HZO in this ortho-IV structure and found that it has a spontaneous polarization of about $60 \mu\text{C}/\text{cm}^2$ and a positive longitudinal piezoresponse $e_{33} = 100 \mu\text{C}/\text{cm}^2$ (the atomistic mechanism for this response is described in Fig. S7 of the Supplementary Information). Hence, a transformation from ortho-IV to ortho-III upon cycling would explain the observed sign reversal in d_{33} . Admittedly, this interpretation is not free of problems. From a theoretical perspective, there are arguments against the possible occurrence of this phase—it has a relatively high bulk energy¹²—but also supporting it—a low surface energy⁵⁴. Then, as far as we know, the ortho-IV phase has never been observed experimentally. Hence, we find the first proposed scenario (continuous evolution between a weakly developed and a well-developed orthorhombic polar phase) more convincing.

Additionally, let us note that it has been recently proposed⁵⁵ that the peculiar behavior of d_{33} observed in HfO_2 (and related compounds) might be related to an intrinsic difficulty in determining the sign of the spontaneous polarization, ultimately caused by the availability of multiple ferroelectric switching paths in these materials. It is unclear whether these ideas may help explain our experiments (for example, they might imply that, upon electric cycling, the dominant switching path in our samples might be changing). Nevertheless, this reinforces the notion that exceptionality of the HfO_2 -based ferroelectrics offers plenty of possibilities for an intrinsic explanation of our experimental results for d_{33} . Let us also stress that none of these scenarios apply to well-known ferroelectrics such as perovskite oxides.

Discussion

While in the literature, some samples exhibit positive d_{33} and other samples exhibit negative d_{33} , we experimentally showed that a complete uniform inversion of the longitudinal piezoelectric coefficient sign can be achieved in the very same $\text{W}/\text{Hf}_{0.5}\text{Zr}_{0.5}\text{O}_2/\text{W}$ ferroelectric capacitor by an electrical ac cycling process. Local PFM switching spectroscopy measurements reveal an evolution, upon ac cycling, from a positive d_{33} value through a continuous reduction of its magnitude down to zero, followed by the d_{33} sign inversion and a gradual increase of the negative d_{33} magnitude. Concomitantly, while the polarization in the pristine state of the capacitors is already relatively large, it keeps increasing well beyond the number of cycles required to uniformly invert the sign of the piezoresponse. Our DFT calculations suggest that a progressive transformation from a weakly developed polar phase to a well-developed o-III phase provides a potential explanation for these observations. Within this model, the non-monotonic development of η_3 with P_3 leads to the unusual behavior of d_{33} , whereby the piezoresponse does not grow with P_3 contrary to what happens in perovskite ferroelectrics. The present results clearly resonate with previous predictions²⁷ that the sign of the piezoresponse of these materials can be tuned, emphasizing that electrical cycling—by controlling the development of the polar distortion—is a key knob for engineering the piezoelectric response of $\text{Hf}_{0.5}\text{Zr}_{0.5}\text{O}_2$ devices. A fine tuning of intermediate states, all the way from a positive ($\sim 3 \text{ pm}/\text{V}$) to negative ($\sim -2 \text{ pm}/\text{V}$) piezoresponse—including a net null one!—can be achieved with ac training while keeping a robust remanent polarization. A next challenge is to find an experimental approach (for example through annealing or mechanical strain) to reversibly change d_{33} back to a positive value. For this purpose, elucidating the role of oxygen ions and oxygen vacancies movement during ac electrical cycling and understanding the interplay between ferroelectricity and ferroionicity would be key^{56,57}. Further investigations are also needed to understand the specific role that the tungsten electrodes seem to play, as the full and uniform d_{33} inversion in the HZO capacitors with TiN electrodes could not be realized so far (although these capacitors exhibit a similar trend, they undergo electrical breakdown before full inversion is reached). Mechanical strain imparted by electrodes (but also by processing conditions, annealing, doping etc.) is a major ingredient for the stabilization of a polar HZO phase and for determining its state evolution towards the fully developed o-III phase (for which a maximum polarization of more than $50 \mu\text{C}/\text{cm}^2$ is predicted by DFT but not yet achieved in polycrystalline films).

With this work, we thus hope to clear the current mystery regarding the sign of piezoelectricity in the HfO_2 -based ferroelectrics by showing that it is not an invariable parameter but a dynamic entity that can be changed in the very same material by an electric field and possibly by other external stimuli. This work also points for the first time to the possible occurrence of an intrinsic non-piezoelectric ferroelectric compound. These findings offer a fantastic playground and unprecedented perspectives to engineer the electromechanical functionality of HfO_2 -based devices.

Methods

Sample and device preparation

Capacitive $\text{W}/\text{HZO}/\text{W}$ stacks were prepared on highly doped p^+ Si substrates. First, a 30 nm-thick W layer was deposited on the silicon substrate by sputtering at room temperature. Then, a 10-nm-thick $\text{Hf}_{0.5}\text{Zr}_{0.5}\text{O}_2$ (HZO) film was grown by atomic layer deposition at 250°C in a FlexAl OXFORD cluster tool using $\text{Hf}(\text{NCH}_3\text{C}_2\text{H}_5)_4$ (TEMAH) and $\text{Zr}(\text{NCH}_3\text{C}_2\text{H}_5)_4$ (TEMAZ) as Hf and Zr precursors respectively and H_2O as an oxidizing agent. HZO was deposited by alternating in a 1:1 ratio the HfO_2 and ZrO_2 cycles except for the two first- and two last cycles, which consisted of HfO_2 . The growth per cycle for this process was $0.15 \text{ nm}/\text{cycle}$. The top 25 nm-thick W

electrodes were prepared in the form of square pads of $95 \times 95 \mu\text{m}^2$ area using a lift-off process with either standard contact photolithography or direct laser lithography and sputtering deposition at room temperature. The capacitive stacks were then annealed using a rapid thermal process at 400°C for 120 s or 180 s under N_2 to crystallize the amorphous HZO films. The low-temperature annealing conditions were chosen for the compatibility of our process with back-end-of-the-line integration of the devices on CMOS chips³⁴. Grazing incidence X-ray diffraction was performed on the pristine stacks with a non-patterned W layer on top (full sheet W deposition and subsequent RTA as similarly described) using Cu K α radiation and an incident angle of 0.5 deg.

A total of five different samples with a minimum of six capacitors per sample were characterized.

Macroscopic electrical measurements

Macroscopic polarization-voltage (P - V) loops were measured in the W/HZO/W capacitors using an arbitrary waveform generator (Keysight 33621 A) for signal generation and an oscilloscope (TDS 3014B, Tektronix) for recording the transient switching currents. A triangular waveform signal at a frequency of 10 kHz was applied to the top electrode via a micromanipulator probe in contact with the top electrode, while the bottom electrode was connected to the oscilloscope for transient current measurements. Subsequent integration of the obtained currents yielded the P - V loops. AC (sine waveform) cycling was performed with an ac voltage of 3 V at 2 kHz.

Further macroscopic P - V loop measurements were carried out using a commercial ferroelectric test system (Radiant Precision Multiferroic II). The field cycling was performed using a sine 1 kHz, ± 2.8 V waveform signal, and the P - V loop measurements were performed using a triangular 1 kHz, ± 3 V. For the measurements of the pristine state, we applied first a preset triangular signal.

PFM imaging and spectroscopy

PFM measurements were performed on a commercial AFM system (MFP3D, Asylum Research) using AFM tips with single crystal diamond probes (D80, K-Tek). Dual AC resonance tracking (DART) PFM mode was used for signal enhancement, where ac drive frequencies near the AFM cantilever contact resonance (~ 360 kHz) and 0.5 V amplitude were applied to the top electrode via an external micromanipulator probe in contact with the electrode, and the AFM tip was used for PFM signal detection. An ac voltage with a 3 V amplitude at 2 kHz was used for ac cycling. All voltages were applied through the external tip, and the PFM tip was used only for the piezoresponse signal detection.

Additional PFM measurements were performed on the capacitors using a Park Systems NX10 microscope. A nonconducting silicon AFM tip (FMR, NanoWorld) was positioned on the top electrode and only detected the electromechanical response of the capacitor. The ac modulation for the PFM measurements was applied to the top electrode through a tungsten needle in contact with it, and other voltage applications, such as ac training cycles and square pulses, were done to the bottom electrode through the highly doped Si substrate. The ac modulation frequency was regulated at ~ 380 kHz by the dual frequency resonance tracking with the lock-in amplifier (UHFLI, Zurich Instruments).

With both scanning probe microscopes, the PFM measurements were performed using top metal electrodes (25 nm thick), which allows us to rule out sample/tip interaction artifacts such as electrostatic charging at the sample surface as a major contribution.

On both set-ups, we used a careful procedure described in ref. 42 to calibrate the PFM phase and to rule out or account for the parasitic effects of any extrinsic phenomena on the measured electro-mechanical response.

First-principles calculations

We perform DFT calculations using the Vienna Ab initio Simulation Package (VASP)^{58,59}. We employ the Perdew-Burke-Ernzerhof formulation for solids (PBEsol)⁶⁰ of the generalized gradient approximation for the exchange-correlation functional. We treat the atomic cores within the projector-augmented wave approach⁶¹, considering the following states explicitly: 5s, 5p, 6s, and 5d for Hf; 4s 4p, 5 s, and 4d for Zr; and 2s and 2p for O. We use a plane-wave energy cut-off of 600 eV for the basis set, which we found to be enough to obtain well-converged results. The Brillouin zone integrals were computed using a $6 \times 6 \times 6$ ($8 \times 6 \times 8$) Monkhorst-Pack⁶² k-point grid for the primitive cell of the o-III and tetragonal (o-IV) phases, corresponding to a simulation cell of 12 (6) atoms. The stable phases were fully relaxed until residual forces fell below 0.001 eV/\AA and residual stresses below 0.01 GPa. The structures along the interpolated path were allowed to relax their lattice vectors until stresses became smaller than 0.01 GPa, keeping their relative atomic coordinates fixed. We obtain the piezoelectric tensor by means of the density functional perturbation theory implementation readily available in VASP⁶³.

Data availability

The data that support the images and plots within this paper and other findings of this study are available from the corresponding authors upon reasonable request.

Code availability

The first-principles simulations were done with VASP, which is proprietary software for which the LIST group owns a license and which can be acquired from the developers (<https://vasp.at/>).

References

1. Böske, T. S., Müller, J., Bräuhaus, D., Schröder, U. & Böttger, U. Ferroelectricity in hafnium oxide thin films. *Appl. Phys. Lett.* **99**, 102903–102903-3 (2011).
2. Schröder, U., Park, M. H., Mikolajick, T. & Hwang, C. S. The fundamentals and applications of ferroelectric HfO₂. *Nat. Rev. Mater.* **7**, 653–669 (2022).
3. Müller, J. et al. Ferroelectricity in simple binary ZrO₂ and HfO₂. *Nano Lett.* **12**, 4318–4323 (2012).
4. Materlik, R., Kuneth, C. & Kersch, A. The origin of ferroelectricity in Hf_{1-x}Zr_xO₂: A computational investigation and a surface energy model. *J. Appl. Phys.* **117**, 134109 (2015).
5. Sang, X., Grimley, E. D., Schenk, T., Schröder, U. & LeBeau, J. M. On the structural origins of ferroelectricity in HfO₂ thin films. *Appl. Phys. Lett.* **106**, 162905 (2015).
6. Shimizu, T. et al. The demonstration of significant ferroelectricity in epitaxial Y-doped HfO₂ film. *Sci. Rep.* **6**, 32931 (2016).
7. Wei, Y. et al. A rhombohedral ferroelectric phase in epitaxially strained Hf_{0.5}Zr_{0.5}O₂ thin films. *Nat. Mater.* **17**, 1095–1100 (2018).
8. Liu, S. & Hanrahan, B. M. Effects of growth orientations and epitaxial strains on phase stability of HfO₂ thin films. *Phys. Rev. Mater.* **3**, 054404 (2019).
9. Lee, H.-J. et al. Scale-free ferroelectricity induced by flat phonon bands in HfO₂. *Science* **369**, 1343–1347 (2020).
10. Yun, Y. et al. Intrinsic ferroelectricity in Y-doped HfO₂ thin films. *Nat. Mater.* **21**, 903–909 (2022).
11. Grimley, E. D. et al. Structural changes underlying field-cycling phenomena in ferroelectric HfO₂ thin films. *Adv. Electron. Mater.* **2**, 1600173 (2016).
12. Huan, T. D., Sharma, V., Rossetti, G. A. Jr & Ramprasad, R. Pathways towards ferroelectricity in hafnia. *Phys. Rev. B* **90**, 064111 (2014).
13. Park, M. H., Kim, H. J., Kim, Y. J., Moon, T. & Hwang, C. S. The effects of crystallographic orientation and strain of thin Hf_{0.5}Zr_{0.5}O₂ film on its ferroelectricity. *Appl. Phys. Lett.* **104**, 072901 (2014).

14. Richter, C. et al. Si doped hafnium oxide—a “fragile” ferroelectric system. *Adv. Electron. Mater.* **3**, 1700131 (2017).
15. Kim, S. J. et al. Large ferroelectric polarization of TiN/Hf_{0.5}Zr_{0.5}O₂/TiN capacitors due to stress-induced crystallization at low thermal budget. *Appl. Phys. Lett.* **111**, 242901 (2017).
16. Schenk, T. et al. On the origin of the large remanent polarization in La:HfO₂. *Adv. Electron. Mater.* **5**, 1900303 (2019).
17. Lomenzo, P. D., Zhao, P., Takmeel, Q., Moghaddam, S. & Nishida, T. Ferroelectric phenomena in Si-doped HfO₂ thin films with TiN and Ir electrodes. *J. Vac. Sci. Technol. B* **32**, 03D123 (2014).
18. Lomenzo, P. D. et al. TaN interface properties and electric field cycling effects on ferroelectric Si-doped HfO₂ thin films. *J. Appl. Phys.* **117**, 134105 (2015).
19. Shimizu, T. et al. Electric-field-induced ferroelectricity in 5%Y-doped Hf_{0.5}Zr_{0.5}O₂: transformation from the paraelectric tetragonal phase to the ferroelectric orthorhombic phase. *Phys. Status Solidi RRL* **15**, 2000589 (2021).
20. Lomenzo, P. D., Richter, C., Mikolajick, T. & Schroeder, U. Depolarization as driving force in antiferroelectric hafnia and ferroelectric wake-up. *ACS Appl. Electron. Mater.* **2**, 1583–1595 (2020).
21. Schroeder, U. et al. Temperature-dependent phase transitions in Hf_xZr_{1-x}O₂ mixed oxides: indications of a proper ferroelectric material. *Adv. Electron. Mater.* **8**, 2200265 (2022).
22. Zhou, S., Zhang, J. & Rappe, A. M. Strain-induced antipolar phase in hafnia stabilizes robust thin-film ferroelectricity. *Sci. Adv.* **8**, eadd5953 (2022).
23. Aramberri, H. & Íñiguez, J. Theoretical approach to ferroelectricity in hafnia and related materials. *arXiv* <https://arxiv.org/abs/2302.00688> (2023).
24. Ding, W., Zhang, Y., Tao, L., Yang, Q. & Zhou, Y. The atomic-scale domain wall structure and motion in HfO₂-based ferroelectrics: a first-principle study. *Acta Mater.* **196**, 556–564 (2020).
25. Liu, J., Liu, S., Liu, L. H., Hanrahan, B. & Pantelides, S. T. Origin of pyroelectricity in ferroelectric HfO₂. *Phys. Rev. Appl.* **12**, 034032 (2019).
26. Liu, J., Liu, S., Yang, J.-Y. & Liu, L. Electric auxetic effect in piezoelectrics. *Phys. Rev. Lett.* **125**, 197601–197601-7 (2020).
27. Dutta, S. et al. Piezoelectricity in hafnia. *Nat. Commun.* **12**, 7301 (2021).
28. Chouprik, A. et al. Nanoscale doping and its impact on the ferroelectric and piezoelectric properties of Hf_{0.5}Zr_{0.5}O₂. *Nanomaterials* **12**, 1483 (2022).
29. Yurchuk, E. et al. Impact of scaling on the performance of HfO₂-based ferroelectric field effect transistors. *IEEE Trans. Electron. Dev.* **61**, 3699–3706 (2014).
30. P. Polakowski, et al. Ferroelectric deep trench capacitors based on Al:HfO₂ for 3D nonvolatile memory applications. In: 2014 IEEE 6th International Memory Workshop (IMW) 1 (2014).
31. McGuire, F. A. et al. Sustained Sub-60 mV/decade switching via the negative capacitance effect in MoS₂ transistors. *Nano Lett.* **17**, 4801–4806 (2017).
32. Chouprik, A. et al. Electron transport across ultrathin ferroelectric Hf_{0.5}Zr_{0.5}O₂ films on Si. *Microelectron. Eng.* **178**, 250–253 (2017).
33. Ambriz-Vargas, F. et al. A complementary metal oxide semiconductor process-compatible ferroelectric tunnel junction. *ACS Appl. Mater. Interfaces* **9**, 13262–13268 (2017).
34. Deshpande, V., Nair, K. S., Holzer, M., Banerjee, S. & Dubourdieu, C. CMOS back-end-of-line compatible ferroelectric tunnel junction devices. *Solid State Electron.* **186**, 108054 (2021).
35. Ryu, H., Wu, H., Rao, F. & Zhu, W. Ferroelectric tunneling junctions based on aluminum oxide/zirconium-doped hafnium oxide for neuromorphic computing. *Sci. Rep.* **9**, 20383 (2019).
36. Max, B., Hoffmann, M., Mulaosmanovic, H., Slesazeck, S. & Mikolajick, T. Hafnia-based double-layer ferroelectric tunnel junctions as artificial synapses for neuromorphic computing. *ACS Appl. Electron. Mater.* **2**, 4023–4033 (2020).
37. E. Covi, et al. Challenges and perspectives for energy-efficient brain-inspired edge computing applications. In: 2022 IEEE International Conference on Flexible and Printable Sensors and Systems (FLEPS), 10–13 July 2022 (2022).
38. Starschich, S., Schenk, T., Schroeder, U. & Boettger, U. Ferroelectric and piezoelectric properties of Hf_{1-x}Zr_xO₂ and pure ZrO₂ films. *Appl. Phys. Lett.* **110**, 182905 (2017).
39. Stolichnov, I. et al. Genuinely ferroelectric sub-1-volt-switchable nanodomains in Hf_xZr_(1-x)O₂ ultrathin capacitors. *ACS Appl. Mater. Interfaces* **10**, 30514–30521 (2018).
40. Collins, L. & Celano, U. Revealing antiferroelectric switching and ferroelectric wakeup in hafnia by advanced piezoresponse force microscopy. *ACS Appl. Mater. Interfaces* **12**, 41659–41665 (2020).
41. Kirbach, S. et al. Doping concentration dependent piezoelectric behavior of Si:HfO₂ thin-films. *Appl. Phys. Lett.* **118**, 012904 (2021).
42. Buragohain, P. et al. Quantification of the electromechanical measurements by piezoresponse force microscopy. *Adv. Mat.* **34**, 2206237 (2022).
43. Gruverman, A., Alexe, M. & Meier, D. Piezoresponse force microscopy and nanoferroic phenomena. *Nat. Commun.* **10**, 1661 (2019).
44. Chouprik, A. et al. Wake-Up in a Hf_{0.5}Zr_{0.5}O₂ film: a cycle-by-cycle emergence of the remnant polarization via the domain depinning and the vanishing of the anomalous polarization switching. *ACS Appl. Electron. Mater.* **1**, 275–287 (2019).
45. Cao, R. et al. Effects of capping electrode on ferroelectric properties of Hf_{0.5}Zr_{0.5}O₂ thin films. *IEEE Electron. Dev. Lett.* **39**, 1207–1210 (2018).
46. Kashir, A., Kim, H., Oh, S. & Hwang, H. Large remnant polarization in a wake-up free Hf_{0.5}Zr_{0.5}O₂ ferroelectric film through bulk and interface engineering. *ACS Appl. Electron. Mater.* **3**, 629–638 (2021).
47. Schenk, T. et al. Electric field cycling behavior of ferroelectric hafnium oxide. *ACS Appl. Mater. Interfaces* **6**, 19744–19751 (2014).
48. Jiang, P. et al. Wake-up effect in HfO₂-based ferroelectric films. *Adv. Electron. Mater.* **7**, 2000728 (2020).
49. Lederer, M. et al. On the origin of wake-up and antiferroelectric-like behavior in ferroelectric hafnium oxide. *Phys. Status Solidi RRL* **15**, 2100086 (2021).
50. Buragohain, P. et al. Nanoscopic studies of domain structure dynamics in ferroelectric La:HfO₂ capacitors. *Appl. Phys. Lett.* **112**, 222901 (2018).
51. Cheng, Y. et al. Reversible transition between the polar and antipolar phases and its implications for wake-up and fatigue in HfO₂-based ferroelectric thin film. *Nat. Comm.* **13**, 645 (2022).
52. Jan, A. et al. In operando optical tracking of oxygen vacancy migration and phase change in few nanometers ferroelectric HZO memories. *Adv. Funct. Mater.* **33**, 2214970 (2023).
53. AzevedoAntunes, L., Ganser, R., Kuenneth, C. & Kersch, A. Characteristics of low-energy phases of hafnia and zirconia from density functional theory calculations. *Phys. Status Solidi RRL* **16**, 2100636 (2022).
54. Batra, R., Tran, H. D. & Ramprasa, R. Stabilization of metastable phases in hafnia owing to surface energy effects. *Appl. Phys. Lett.* **108**, 172902 (2016).
55. Y. Qi, S. E. Reyes-Lillo, K. M. Rabe. Double-path” ferroelectrics and the sign of the piezoelectric response. <https://arxiv.org/abs/2204.06999> (2022).
56. P. D. Lomenzo et al. Discovery of nanoscale electric field-induced phase transitions in ZrO₂. *Adv. Funct. Mater.* 2303636 (2023).
57. Kelley, K. P. et al. Ferroelectricity in hafnia controlled via surface electrochemical state. *Nat. Mater.* **22**, 1144–1151 (2023).

58. Kresse, G. & Furthmüller Efficient iterative schemes for ab initio total-energy calculations using a plane-wave basis set. *Phys. Rev. B* **54**, 11169–11186 (1996).
59. Kresse, G. & Joubert, D. From ultrasoft pseudopotentials to the projector augmented-wave method. *Phys. Rev. B* **59**, 1758–1775 (1999).
60. Perdew, J. P. et al. Restoring the density-gradient expansion for exchange in solids and surfaces. *Phys. Rev. Lett.* **100**, 136406–136406-4 (2008).
61. Blöchl, P. E. Projector augmented-wave method. *Phys. Rev. B* **50**, 17953–17979 (1994).
62. Monkhorst, H. J. & Pack, J. D. Special points for Brillouin-zone integrations. *Phys. Rev. B* **13**, 5188–5192 (1976).
63. Wu, X., Vanderbilt, D. & Hamann, D. R. Systematic treatment of displacements, strains, and electric fields in density-functional perturbation theory. *Phys. Rev. B* **72**, 035105–035105-13 (2005).

Acknowledgements

C.D., D.-J.K., V.D., and M.H. acknowledge funding by Horizon 2020 EU project BeFerroSynaptic (No. 871737). C.D. and D.-J.K. acknowledge the funding and cooperation from Park Systems. Dr. H. Raza from HZB is acknowledged for growing additional samples. K. S. Nair and T.L. Phan, PhD, are acknowledged for performing lithography. Work at LIST (H.A., J.Í.) was funded by the Luxembourg National Research Fund through grant INTER/NWO/20/15079143/TRICOLOR. A.G. and C.D. acknowledge the support of the Alexander von Humboldt Foundation.

Author contributions

C.D. initiated and coordinated the study. C.D. and A.G. supervised the experimental work. M.H. grew the samples and performed electrical measurements on the capacitors. H.L., with the assistance of P.B. and D.J.K., performed the PFM and macroscopic electrical measurements of the capacitors. H.A. performed the first-principles study, assisted by S.D. and supervised by J.Í. C.D., A.G., J.Í., H.L., D.J.K., H.A., M.H., P.B., S.D., U.S., and V. D. discussed the results. The manuscript was written by C.D., A.G., J.Í., D.J.K., and H.L. with contributions from H.A. All co-authors edited the manuscript.

Funding

Open Access funding enabled and organized by Projekt DEAL.

Competing interests

The authors declare no competing interests.

Additional information

Supplementary information The online version contains supplementary material available at <https://doi.org/10.1038/s41467-024-44690-9>.

Correspondence and requests for materials should be addressed to Jorge. Íñiguez, Alexei Gruverman or Catherine Dubourdieu.

Peer review information *Nature Communications* thanks Ignasi Fina and the other anonymous reviewer(s) for their contribution to the peer review of this work. A peer review file is available.

Reprints and permissions information is available at <http://www.nature.com/reprints>

Publisher's note Springer Nature remains neutral with regard to jurisdictional claims in published maps and institutional affiliations.

Open Access This article is licensed under a Creative Commons Attribution 4.0 International License, which permits use, sharing, adaptation, distribution and reproduction in any medium or format, as long as you give appropriate credit to the original author(s) and the source, provide a link to the Creative Commons license, and indicate if changes were made. The images or other third party material in this article are included in the article's Creative Commons license, unless indicated otherwise in a credit line to the material. If material is not included in the article's Creative Commons license and your intended use is not permitted by statutory regulation or exceeds the permitted use, you will need to obtain permission directly from the copyright holder. To view a copy of this license, visit <http://creativecommons.org/licenses/by/4.0/>.

© The Author(s) 2024